XPS studies on the interaction of CeO_2 with Silicon in magnetron sputtered CeO_2 thin films on Si and Si_3N_4 substrates

C. Anandan* and Parthasarathi Bera
Surface Engineering Division, CSIR–National Aerospace Laboratories,
Post Bag No. 1779, HAL Airport Road,
Bangalore 560017, India

Abstract

CeO_2 thin films were deposited on silicon and silicon nitride substrates by magnetron sputtering at room temperature and annealed at 400 and 600 °C in air and vacuum. Interaction between deposited CeO_2 and Si in CeO_2/Si and CeO_2/Si_3N_4 systems was investigated by XPS. The results show that Ce is present as both Ce^{4+} and Ce^{3+} oxidation states in CeO_2 film deposited on Si substrate, whereas Ce^{4+} is the main species in as-deposited CeO_2/Si_3N_4 film. Detailed analyses of Ce3d, Si2p and O1s core level spectra demonstrate that Ce_2O_3 and SiO_x or cerium silicate type of species are formed at the interface of CeO_2 and Si. Concentrations of Ce^{3+} species increase drastically in CeO_2/Si thin films after annealing at 400 °C in vacuum due to enhanced interfacial reaction. On the other hand, interfacial reaction between CeO_2 and Si_3N_4 substrate is limited in as-deposited as well as 600 °C heat treated films.

Keywords: CeO_2; Thin film; Silicon; Silicon nitride; Interfacial reaction; XPS

*Corresponding author, E mail: canandan@nal.res.in

Fax: +91–080–25210113

1. Introduction

In last several years, CeO_2 powders and thin films have become attractive materials for various catalytic, electrochemical, electronic, optical, electrical, gas sensor and corrosion resistant applications [1–8]. CeO_2 based materials are important for applications in auto exhaust catalysis, hydrogen production, electrodes in fuel cells [1,2,9,10]. In microelectronics, among various high-κ gate oxide materials, CeO_2 is one of the attractive candidates due to its high dielectric constant (23–52), high refractive index (2.2–2.8), high dielectric strength (~25 MV cm^{-1}) and moderate band gap (3–3.6 eV) [11]. Small lattice mismatch as well as thermodynamic stability in contact with Si favors the epitaxial growth of CeO_2 on different Si surfaces [12,13]. Moreover, with its good adhesion on Si, high stability against mechanical abrasion and chemical attack it is more suitable for complementary metal–oxide–semiconductor (CMOS) devices. It has also been a potential alternative to standard SiO_2 based silicon-on-insulator (SOI) technology [14]. In this sense, many research groups have attempted to grow epitaxial thin films on Si substrates by different thin film deposition techniques such as electron beam evaporation, magnetron sputtering, flash evaporation, pulsed laser deposition, ion beam epitaxy, molecular beam epitaxy, plasma enhanced chemical vapor deposition, sol-gel, spray pyrolysis [12–24]. However, in most cases, an important issue is the nature of CeO_2–Si interface and its stability as potential applications depend on better understanding and controlling the quality of CeO_2/Si interface.

It has been found that Si can react with CeO_2 at the CeO_2/Si interface to form silicon oxides, cerium silicate [13,19,25–27]. In a recent study, Skála and Matolín have investigated the interaction of silicon and CeO_2 employing XPS where they have found the formation of cerium

silicate whose thickness has been limited by diffusion of silicon [28]. They have also found formation of sub oxides of silicon. When CeO_2 is directly deposited on Si, an interfacial layer is formed resulting in high interface state densities and in an increase of effective oxide thickness which is not desirable [18,25]. For example, silicate and silicide formed at the interface of high-κ material, HfO_2 and Si during film deposition and subsequent annealing has been found to degrade the device performance [29–31]. However, Si_3N_4 layer has been used to minimize the formation of interfacial layers in case of HfO_2/Si film [32,33]. Interfacial reaction with HfO_2 has been controlled by nitridation and oxynitridation of Si [30]. Therefore, within this context, interaction between CeO_2 and Si_3N_4 is important. Hence, thermal stability and bonding nature at the interface of CeO_2 and Si in CeO_2/Si and CeO_2/Si_3N_4 has been explored in details in this work.

Growth of CeO_2 on Si substrate, their structure and interaction with Si under different conditions have been studied by XRD, TEM, SEM, RHEED, LEED, RBS, Raman, AES, XPS and XANES [15,16,18,20,34–38]. XPS particularly provides detailed information about the electronic nature of the interaction. There are several XPS studies about the interfacial reaction between CeO_2 and Si in the literature [13,25,26,38–42]. However, growth and structure of CeO_2 on Si_3N_4 substrate and their interaction is lacking in the literature. In the present study, we, for the first time report the growth of CeO_2 on Si_3N_4 substrate using magnetron sputtering and detailed XPS studies of interaction between CeO_2 and Si. Growth and interaction of CeO_2 with Si on Si substrate have also been investigated for comparison.

2. Experimental methods

CeO_2 thin films were deposited on Si and Si_3N_4 substrates using a CeO_2 target (Allvac, 99.9%) employing magnetron sputtering assisted by inductively coupled plasma generated with

50 W RF power at 13.56 MHz. The substrates were cleaned by sonication using acetone/isopropyl alcohol prior to loading into the vacuum chamber. The chamber was pumped down to a base pressure of 3×10^{-6} mbar. The substrates were etched with H_2 plasma prior to deposition of thin films. Sputter deposition was carried out at room temperature with Ar atmosphere at a pressure of 8 μbar. The substrate was biased to a constant negative voltage of 150 V and the target was biased with bipolar pulses of 300 V using a pulse generator. Thickness of obtained CeO_2 thin films is around 25 nm.

XPS of CeO_2 thin films were recorded with a SPECS spectrometer using non-monochromatic AlKα source (1486.6 eV) run at 150 W (12 kV and 12.5 mA). The binding energies reported here were calculated with reference to C1s peak at 284.6 eV with a precision of ± 0.1 eV. All the spectra were obtained with a pass energy of 25 eV and step increment of 0.05 eV. The experimental data were curve fitted into several components with Gaussian-Lorentzian peaks using Shirley background employing CasaXPS program. For component peaks, slightly different full width at half maximum (FWHM) was used for different chemical states. The spin-orbit splitting and doublet intensities were fixed as given in the literature [43].

3. Results and discussion

3.1. As-deposited films

Fig. 1 compares Ce3d core level spectra of CeO_2 films deposited on Si and Si_3N_4 substrates. The spectral envelop of Ce3d on Si substrate reveals that Ce is in both +4 and +3 oxidation states and it could be resolved into several $Ce3d_{5/2,3/2}$ spin-orbit doublet peaks with splitting of around 18 eV. In contrast, on Si_3N_4 substrate, the spectrum mostly resembles the +4 state in CeO_2. Fig. 2 presents deconvoluted Ce3d spectra of CeO_2 coated on Si and Si_3N_4 substrates. Binding energies, FWHMs and relative integrated peak areas of $Ce3d_{5/2,3/2}$ spin-orbit

doublets in CeO_2 films deposited on Si and Si_3N_4 are summarized in Tables 1 and 2, respectively. In Fig. 2 (a) related to CeO_2/Si film, peaks labeled as v are arising from $3d_{5/2}$ photoemissions, whereas associated $3d_{3/2}$ emissions are labeled as u. Spin-orbit peaks of v‴ and u‴ at 898.2 and 916.5 eV with 18.3 eV separation are attributed to primary photoionization from Ce^{4+} with $Ce3d^94f^0O2p^6$ final state. Lower binding energy states of v″–u″ and v–u have been assigned to the $Ce3d^94f^1O2p^5$ and $Ce3d^94f^2O2p^4$ final states shake-down satellite features [38,44–47]. Satellites are caused by the facilitation of ligand (O2p) to metal (Ce4f) charge transfer by primary photoionization process. Peaks labeled as v_o, v′ and u_o, u′ at 881.1, 885.5 and 899.0, 903.9 eV are associated with Ce^{3+} final states. In this sense, v′–u′ spin orbit doublet peaks are assigned to main photoionization from $Ce3d^94f^1O2p^6$ final state, whereas lower binding energy v_o–u_o peaks correspond to characteristic $Ce3d^94f^2O2p^5$ final state shake-down satellites [26,38,44–48]. It has been proposed that fully oxidized CeO_2 layer grows on top of the interfacial phase and Ce^{3+} containing phase is buried under CeO_2 layer [13]. Peak areas (A) of Ce^{4+} and Ce^{3+} components are commonly used to estimate their relative concentrations (C) in the films using the following equations [26,46]:

$$A_{Ce^{3+}} = A_{v_o} + A_{u_o} + A_{v'} + A_{u'} \quad (1)$$

$$A_{Ce^{4+}} = A_{v} + A_{u} + A_{v''} + A_{u'''} + A_{v'''} + A_{u'''} \quad (2)$$

$$C_{Ce^{3+}} = \frac{A_{Ce^{3+}}}{A_{Ce^{4+}} + A_{Ce^{3+}}} \quad (3).$$

According to the equation (3) the concentration of Ce^{3+} in CeO_2 deposited on Si is estimated to be 32% with respect to the total amount of Ce species. On the other hand, mainly Ce^{4+} related peaks along with a small amount of Ce^{3+} can be seen in CeO_2 deposited on Si_3N_4 substrate which

is displayed in Fig. 2 (b). Here estimated amount of Ce^{3+} is 11% only. It is worth noting that Ce is in +3 oxidation state in all cerium silicates and therefore, observation of Ce^{3+} in CeO_2 films deposited on both Si and Si_3N_4 substrates can be associated with formation of cerium silicate as observed in similar CeO_2 films or Ce_2O_3 at the interface [13]. It is to be noted that amount of Ce^{3+} is less on Si_3N_4 substrate in comparison with Si substrate indicating that interfacial reaction between CeO_2 and Si is low when CeO_2 is deposited on Si_3N_4 substrate.

In Fig. 3, Si2p core level spectra from Si substrate coated with CeO_2 film is shown. Si2p in pure Si substrate is also given for comparison. A sharp peak at 99.4 eV observed in pure Si substrate corresponds to elemental Si. In contrast, broad nature of Si2p core level spectrum in CeO_2 coated Si substrate indicates the presence of several Si species which can be deconvoluted into component peaks. Component peak at 99.3 eV corresponds to elemental Si present in Si substrate, whereas peaks observed at 101.2 and 102.4 eV could be attributed to Si^{2+} and Si^{3+} species [49,50]. The appearance of these species at the interface of CeO_2 and Si shows the interaction between them where it can be expected to bond in a Si–Ce–O matrix in the form of silicate [27]. On the other hand, single peak at 101.5 eV found in Si2p core level spectrum in CeO_2/Si_3N_4 film can be assigned for Si–N bond in Si_3N_4 [51].

O1s core level spectra can be used as another source of information on oxidation states of Ce. Deconvoluted O1s core level spectra from as-deposited film on Si and Si_3N_4 substrates are shown in Fig. 4. O1s core level spectrum in as-deposited film on Si shows four peaks at 529.9, 531.6, 532.1 and 533.8 eV (Fig. 4a). Peak at 529.9 eV can be attributed to O^{2-} species in CeO_2, whereas observed peak at 532.1 eV corresponds to O in Si–O bonded species that compares well with the literature [13,40,41]. Intermediate peak at 531.6 eV is related to Ce^{3+} species originated from silicate or Ce_2O_3 species [13]. Amount of Ce^{3+} has been estimated from areas of O1s

component peaks related to Ce^{4+} and Ce^{3+} species and it is found to be 28% which is close to the estimation from corresponding Ce3d peak. A higher binding energy component at 533.8 eV is associated with adsorbed H_2O species. In contrast, CeO_2 film deposited on Si_3N_4 substrate contains an intense peak at 529.8 eV that is related to O^{2-} species in CeO_2 (Fig. 4b). Two weak peaks at 531.4 and 532.5 eV are assigned for oxygen species in silicate or Ce_2O_3 and Si–O network, respectively. Thus, O1s core levels demonstrate that the relative concentration of Ce^{3+} related oxygen species is less in the film deposited on Si_3N_4 substrate compared with Si counterpart.

3.2. Heat treated films

CeO_2 films on Si and Si_3N_4 substrates were heat treated at 400 and 600 °C under a vacuum of 10^{-5} mbar for 30 min to know about the stability of the interface. Films coated on Si_3N_4 substrate were also heated at the same temperatures in air, but in case of films on Si, only vacuum annealing was carried out to avoid effect of atmospheric oxygen. Fig. 5 compares Ce3d core level spectra from CeO_2 deposited on Si and Si_3N_4 after annealing at different conditions. It can be observed from the figure that Ce3d spectral nature on Si substrate heated at 400 and 600 °C in vacuum are different from that on Si_3N_4 substrate. Amount of Ce^{4+} species in CeO_2 films deposited on Si substrate decreases when films are heat treated at higher temperatures indicating the reduction of Ce^{4+} species. This can be clearly understood from the intensity of u′′′ peak that decreases on annealing. After annealing the film at 600 °C in vacuum, u′′′ peak nearly disappears in the Ce3d spectrum shown in Fig. 5. Typical deconvoluted Ce3d core level spectra from 400 and 600 °C heat treated CeO_2 coated on Si and Si_3N_4 substrates, respectively are given in Fig. 6. Deconvoluted spectrum of the CeO_2/Si film heated at 400 °C in vacuum shown in Fig. 6 (a)

demonstrates the presence of mainly Ce^{3+} species in heat treated film and its amount is 54% calculated using equation (3). Peaks labeled as v_o, v′ and u_o, u′ at 881.5, 885.6 and 899.4, 904.2 eV are assigned to Ce^{3+} final states along with small contributions from Ce^{4+} species at 883.2, 888.5, 898.4, 901.6, 906.7 and 916.8 eV. Ce^{3+} species can be related to the formation of silicate or Ce_2O_3 like phases. Intensities of peaks associated with Ce^{4+} species further decrease when sample is vacuum heated at 600 °C and from Fig. 5 it is clear that film predominately contains Ce^{3+} species. Amount of Ce^{3+} is 74% as evaluated from deconvoluted spectrum. In contrast, Ce^{4+} species predominates in CeO_2/Si_3N_4 films heated at 400 and 600 °C in vacuum and also in air as can be seen from the intensity of u′′′ peak in Fig. 5 as well as the deconvoluted Ce3d spectrum in Fig. 6 (b) related to CeO_2/Si_3N_4 film heated at 600 °C. Though concentration of Ce^{3+} species increases slightly in CeO_2/Si_3N_4 film when heat treatment temperature increases from 400 to 600 °C in vacuum, but overall predominant species is Ce^{4+}. Similarly, Ce^{4+} is the main species in CeO_2/Si_3N_4 films heated at 400 and 600 °C in air along with trace amount of Ce^{3+} components that could be seen from Tables 3 and 4, respectively where binding energies and relative integrated peak areas of $Ce3d_{5/2,3/2}$ spin-orbit doublets are given. This shows that CeO_2/Si_3N_4 film is stable even after high temperature heat treatment in air. Similar characteristic behavior has also been reflected in the Ce4d core level spectra of as-deposited and heat treated films which are shown in Fig. 7. Ce4d core level of as-deposited CeO_2/Si thin film shows several peaks at 108.5, 111.8, 114.8, 121.7 and 125.0 eV. According to the literature, peaks at 121.7 and 125.0 eV with spin-orbit splitting of 3.3 eV correspond to $Ce4d_{5/2,3/2}$ components of Ce^{4+} [52,53]. It is clear from the Fig. 7 that as-deposited CeO_2 film on Si substrate contains lower amount of Ce^{4+} species and it further decreases with increase in heat treatment temperature. On the other hand, intense higher binding energy Ce^{4+} component peaks are observed in the spectra obtained

from as-deposited as well as heat treated CeO_2 films deposited on Si_3N_4 substrate. Thus, XPS results demonstrate that heat treatment of CeO_2 films deposited on Si substrate facilitates the interfacial reaction between CeO_2 and Si resulting cerium silicate or Ce_2O_3. In contrast, the interface between CeO_2 and Si_3N_4 is stable even after high temperature treatment in air and vacuum.

Deconvoluted Si2p core level spectra from Si substrate obtained after heat treatment at 400 and 600 °C in vacuum are shown in Fig. 8. Envelop of Si2p core level peak in heat treated films on Si in the figure indicates an increase in spectral intensities of oxide related peaks already present in the as-deposited condition. Peaks at 99.3, 101.2 and 102.3 eV are assigned for elemental Si^0, Si^{2+} and Si^{3+} species, respectively. A new peak at 103.3 eV is also seen along with the other three peaks in the film heated at 600 °C that is related to Si^{4+} species [49,50]. New species are formed at the interface of CeO_2 and Si due to enhanced interaction between them at higher temperatures. On the other hand, Si2p core level spectral features in CeO_2/Si_3N_4 films with various heat treatment conditions shown in Fig. 9 are different from CeO_2/Si films. Si2p spectrum from pure Si_3N_4 substrate is also shown in the figure for comparison. In Si_3N_4 substrate, Si2p peak at 101.5 eV is assigned for Si–N bond in Si_3N_4 which agrees well with the literature [51]. A single peak at 101.7 eV corresponding to Si2p is observed in as-deposited as well as vacuum annealed CeO_2/Si_3N_4 films. The intensity of this peak is very low in air annealed CeO_2/Si_3N_4 films.

O1s spectral features have changed due to annealing of CeO_2 films on both substrates and they are shown in Fig. 10. It is clear from Fig. 10 (a) that intensity of O1s component associated with CeO_2 in CeO_2/Si film is reduced after heat treatment at 400 °C in vacuum, whereas intensity of Ce_2O_3 related peak at 532 eV increases. Concentration of Ce^{3+} species evaluated from the

deconvoluted O1s core level spectrum increases to 56% after annealing at 400 °C in vacuum which is close to the value of 54% obtained from Ce3d spectrum. On the other hand, CeO_2 film deposited on Si_3N_4 substrate shows an intense peak at 529.9 eV corresponding to O^{2-} species in CeO_2 after heat treatment at 400 °C in vacuum as displayed in Fig. 10 (b). Two low intensity peaks at 531.7 and 532.9 eV are attributed to oxygen species in silicate or Ce_2O_3 and Si–O network, respectively. Relative concentration of Ce^{3+} from O1s core level peak of CeO_2/Si_3N_4 heat treated at 400 °C in vacuum is 14% which is close to the value of 15% obtained from Ce3d spectrum. Ce^{3+} concentration increases slightly upon heat treatment at 600 °C. However, concentrations of Ce^{4+} and Ce^{3+} in CeO_2/Si_3N_4 films after heat treatment in air are more or less same with as-deposited film. Thus, XPS studies demonstrate the stability of CeO_2/Si_3N_4 interface and that there is no significant change in concentrations of Ce^{4+} and Ce^{3+} in CeO_2 films on Si_3N_4 substrate after heat treatment in air or vacuum.

In this work, XPS studies of CeO_2 films coated on Si and Si_3N_4 substrates demonstrate the presence of Ce_2O_3 and silicate phase at the interface between CeO_2 and Si at room temperature. Reactivity at the interface appears to be absent when CeO_2 is deposited on Si_3N_4 substrate. Extent of interfacial reaction increases with Si after heat treatment but it is minimum in case of Si_3N_4. Si has unfilled p level, whereas Si_3N_4 is an insulator with a large band gap of 5.1 eV having filled p levels of Si. In this sense, Si present on the silicon surface reacts with deposited CeO_2 layer in CeO_2/Si film and the interfacial reactions can be written as follows:

$$3Si + 8CeO_2 \rightarrow SiO + Si_2O_3 + 4Ce_2O_3 + 283.2\ kJ\ mol^{-1} \qquad (4).$$

Thus, from thermodynamic point of view, the interfacial reaction given above can occur in the forward direction if we consider standard molar enthalpy of formation of different compounds. Another type of reaction between Si and CeO_2 is also possible which is given below.

$$x\mathrm{Si} + \mathrm{CeO_2} \rightarrow \mathrm{CeSi}_x\mathrm{O}_y + \mathrm{CeO}_{2-y} \qquad (5).$$

A similar type of silicate phase has also been found at HfO_2/Si interface [29,33]. Another way of understanding the results would be position of valence bands. Si^0 and Si_3N_4 have valence bands starting at 0.95 and 3.7 eV, respectively with respect to Fermi level, whereas empty Ce4f band in CeO_2 is located at 2 eV [54,55,2]. Therefore, Si^0 can transfer its electron easily to CeO_2 in CeO_2/Si film that facilitates reduction of Ce^{4+} to Ce^{3+}. On the other hand, possibility of this kind of electron transfer in CeO_2/Si_3N_4 film is much less as valence band of Si_3N_4 is situated on the lower energy side compared to empty Ce4f band according to Fermi level. Therefore, interfacial reaction is absent in CeO_2/Si_3N_4 film.

Conclusions

CeO_2 films were deposited on Si and Si_3N_4 substrates by magnetron sputtering. XPS studies show that significant amount of Ce^{3+} is present in addition to Ce^{4+} in CeO_2/Si films due to interaction between CeO_2 and silicon on silicon substrate. Mainly Ce^{4+} species are observed in as-deposited CeO_2/Si_3N_4 films. Interfacial reaction between CeO_2 and Si leads to the silicate formation. Heat treatment enhances the interfacial reaction in CeO_2/Si films. On the other hand, Ce^{4+} species predominates in CeO_2/Si_3N_4 films even after heat treatment at high temperatures in vacuum and air demonstrating the stability of the interface.

Acknowledgments

Authors would like to thank the Director, CSIR–National Aerospace Laboratories for giving permission to publish this work and Prof. M. S. Hegde, Emiretus Professor, Indian Institute of Science, Bangalore for fruitful discussion.

References

[1] A. Trovarelli, Catalysis by Ceria and Related Materials, Imperial College Press, London, 2002.

[2] P. Bera, M.S. Hegde, Catal. Surv. Asia 15 (2011) 181.

[3] M. Mogensen, N.M. Sammes, G.A. Tompsett, Solid State Ionics 129 (2000) 63.

[4] H. Inaba, H. Tagawa, Solid State Ionics 83 (1996) 1.

[5] R.M. Bueno, J.M. Martinez-Duart, M. Hernández-Vélez, L. Vázquez, J. Mater. Sci. 32 (1997) 1861.

[6] M.R. Mohammadi, D.J. Fray, Sens. Actuator B 150 (2010) 631.

[7] X. Zhong, Q. Li, J. Hu, Y. Lu, Corros. Sci. 50 (2008) 2304.

[8] A. Samide, B. Tutunaru, Chem. Biochem. Eng. Quarterly 25 (2011) 203.

[9] P.Y. Sheng, W.W. Chiu, A. Yee, S.J. Morrison, H. Idriss, Catal. Today 129 (2007) 313.

[10] M. Václavů, I. Matolínová, J. Mysliveček, R. Fiala, V. Matolín, J. Electrochem. Soc. 156 (2009) B938.

[11] W.-H. Kim, W.J. Maeng, M.-K. Kim, J. Gatineau, H. Kim, J. Electrochem. Soc. 158 (2011) G217.

[12] J.C. Wang, K.C. Chiang, T.F. Lei, C.L. Lee, Electrochem. Solid State Lett. 7 (2004) E55.

[13] F. Pagliuca, P. Luches, S. Valeri, Surf. Sci. 607 (2013) 164.

[14] T. Chikyow, S. M. Bedair, L. Tye, N. A. El-Masry, Appl. Phys. Lett. 65 (1994) 1030.

[15] I. Porqueras, C. Person, C. Corbella, M. Vives, A. Pinyol, E. Bertran, Solid State Ionics 165 (2003) 131.

[16] L. Kim, J. Kim, D. Jung, C.-Y. Park, C.-W. Yang, Y. Roh, Thin Solid Films 360 (2000) 154.

[17] M.-T. Ta, D. Briand, Y. Guhel, J. Bernard, J.C. Pesant, B. Boudart, Thin Solid Films 517 (2008) 450.

[18] A. Ramírez-Duverger, A.R. Ruiz-Salvador, M.P. Hernández-Sánchez, M.F. García-Sánchez, G. Rodríguez-Gattorno, Solid State Ionics 96 (1997) 89.

[19] B. Hirschauer, G. Chiaia, M. Göthelid, U.O. Karlsson, Thin Solid Films 348 (1999) 3.

[20] D. Huang, F. Qin, Z. Yao, Z. Ren, L. Lin, W. Gao, Q. Ren, Appl. Phys. Lett. 67 (1995) 3724.

[21] J.T. Jones, E.T. Croke, C.M. Garland, O.J. Marsh, T.C. McGill, J. Vac. Sci. Technol. B 16 (1998) 2686.

[22] D. Barreca, G. Bruno, A. Gasparotto, M. Losurdo, E. Tondello, Mater. Sci. Eng. C 23 (2003) 1013.

[23] N. Özer, Solar Energy Mater. Solar Cells 68 (2001) 391.

[24] S. Wang, W. Wang, Q. Liu, M. Zhang, Y. Qian, Solid State Ionics 133 (2000) 211.

[25] C.E. Guillaume, M. Vermeersch, J.J. Verbist, S. Mathot, G. Demortier, Surf. Interface Anal. 22 (1994) 186.

[26] E.J. Preisler, O.J. Marsh, R.A. Beach, T.C. McGill, J. Vac. Sci. Technol. B 19 (2001) 1611.

[27] R. Barnes, D. Starodub, T. Gustafsson, E. Garfunkel, J. Appl. Phys. 100 (2006) 044103.

[28] T. Skála, V. Matolín, Appl. Surf. Sci. 265 (2013) 817.

[29] H. Wong, N. Zhan, K.L. Ng, M.C. Poon, C.W. Kok, Thin Solid Films 462–463 (2004) 96.

[30] R. Katamreddy, R. Inman, G. Jursich, A. Soulet, C. Takoudis, Thin Solid Films 516 (2008) 8498.

[31] H. Wang, P. Wu, X.F. Li, S. Chen, S.P. Zhang, B.B. Song, Appl. Surf. Sci. 257 (2011) 3440.

[32] H. Kobayashi, K. Imamura, K. Fukayama, S.-S. Im, O. Maida, Y.-B. Kim, H.-C. Kim, D.-K. Choi, Surf. Sci. 602 (2008) 1948.

[33] P.D. Kirsch, C.S. Kang, J. Lozano, J.C. Lee, J.G. Ekerdt, J. Appl. Phys. 91 (2002) 4353.

[34] J. de Souza, A.G.P. da Silva, H.R. Paes, Jr., J. Mater. Sci. Mater. Electron 18 (2007) 951.

[35] H.-Y. Lee, S.-I. Kim, Y.-P. Hong, Y.-C. Lee, Y.-H. Park, K.-H. Ko, Surf. Coat. Technol. 173 (2003) 224.

[36] C. Hardacre, G.M. Roe, R.M. Lambert, Surf. Sci. 326 (1995) 1.

[37] T. Inoue, Y.Yamamoto, S. Koyama, S. Suzuki, Y. Ueda, Appl. Phys. Lett. 56 (1990) 1332.

[38] V. Fernandes, I.L. Graff, J. Varald, L. Amaral, P. Fichtner, D. Demaille, Y. Zheng, W.H. Schreiner, D.H. Mosca, J. Electrochem. Soc. 159 (2012) K27.

[38] Z. Wu, D. Huang, J. Wang, F. Qin, J. Zhang, Z. Yang, Vacuum 49 (1998) 133.

[40] B. Hirschauer, M. Göthelid, E. Janin, H. Lu, U.O. Karlsson, Appl. Surf. Sci. 148 (1999) 164.

[41] C.G. Kim, J. Vac. Sci. Technol. B, 18 (2000) 2650.

[42] W.-H. Kim, M.-K. Kim, W.J. Maeng, J. Gatineau, V. Pallem, C. Dussarrat, A. Noori, D. Thompson, S. Chu, H. Kim, J. Electrochem. Soc. 158 (2011) G169.

[43] D. Briggs, M.P. Seah, Practical Surface Analysis by Auger and X-ray Photoelectron Spectroscopy, Wiley, New York, 1984.

[44] A. Pfau, K.D. Schierbaum, Surf. Sci. 321 (1994) 71.

[45] D.R. Mullins, S.H. Overbury, D.R. Huntley, Surf. Sci. 409 (1998) 307.

[46] V. Chauvaut, V. Albin, H. Schneider, M. Cassir, H. Ardéléan, A. Galtayries, J. Appl. Electrochem. 30 (2000) 1405.

[47] E. Bêche, P. Charvin, D. Perarnau, S. Abanades, G. Flamant, Surf. Interface Anal. 40 (2008) 264.

[48] Y. Zhou, J.M. Perket, J. Zhou, J. Phys. Chem. C 114 (2010) 11853.

[49] G. Hollinger, F.J. Himpsel, Appl. Phys. Lett. 44 (1984) 93.

[50] J.R. Shallenberger, J. Vac. Sci. Technol. A 14 (1996) 693.

[51] S.I. Raider, R. Flitsch, J.A. Aboaf, W.A. Pliskin, J. Electrochem. Soc. 123 (1976) 560.

[52] E. Paparazzo, G.M. Ingo, Z. Zachhetti, J. Vac. Sci. Technol. A 9 (1991) 1416.

[53] W. Xiao, Q. Guo, E.G. Wang, Chem. Phys. Lett. 368 (2003) 527.

[54] A. Bahari, P. Morgen, Z. S. Li, Surf. Sci. 600 (2006) 2966.

[55] C. Sénémaud, M. Driss-Khodja, A. Gheorghiu, S. Harel, G. Dufour, H. Roulet, J. Appl. Phys. 74 (1993) 5042.

Table 1 Binding energies and integrated peak areas of $Ce3d_{5/2,3/2}$ spin-orbit doublets in CeO_2 film deposited on Si.

Peak assignment	Ce species	Binding energy (eV)	Relative area (%)
v_o	Ce^{3+}	881.1	6
v	Ce^{4+}	882.8	15
v′	Ce^{3+}	885.5	14
v″	Ce^{4+}	888.8	11
v‴	Ce^{4+}	898.2	13
u_o	Ce^{3+}	899.0	4
u	Ce^{4+}	901.2	12
u′	Ce^{3+}	903.9	8
u″	Ce^{4+}	907.0	9
u‴	Ce^{4+}	916.5	10

Table 2 Binding energies and integrated peak areas of $Ce3d_{5/2,3/2}$ spin-orbit doublets in CeO_2 film deposited on Si_3N_4.

Peak assignment	Ce species	Binding energy (eV)	Relative area (%)
v_o	Ce^{3+}	881.2	3
v	Ce^{4+}	882.7	20
v′	Ce^{3+}	885.4	5
v″	Ce^{4+}	888.9	14
v‴	Ce^{4+}	898.4	20
u_o	Ce^{3+}	899.3	1
u	Ce^{4+}	901.2	11
u′	Ce^{3+}	903.9	2
u″	Ce^{4+}	907.4	8
u‴	Ce^{4+}	916.7	16

Table 3 Binding energies and integrated peak areas of $Ce3d_{5/2,3/2}$ spin-orbit doublets in CeO_2 film deposited on Si_3N_4 and heat treated at 400 °C in air.

Peak assignment	Ce species	Binding energy (eV)	Relative area (%)
v_o	Ce^{3+}	881.5	3
v	Ce^{4+}	882.3	21
v′	Ce^{3+}	885.4	4
v″	Ce^{4+}	888.8	16
v‴	Ce^{4+}	898.1	19
u_o	Ce^{3+}	899.2	1
u	Ce^{4+}	900.7	11
u′	Ce^{3+}	903.4	2
u″	Ce^{4+}	907.5	7
u‴	Ce^{4+}	916.4	16

Table 4 Binding energies and integrated peak areas of $Ce3d_{5/2,3/2}$ spin-orbit doublets in CeO_2 film deposited on Si_3N_4 and heat treated at 600 °C in air**.**

Peak assignment	Ce species	Binding energy (eV)	Relative area (%)
v_o	Ce^{3+}	881.2	3
v	Ce^{4+}	882.4	21
v′	Ce^{3+}	885.2	4
v″	Ce^{4+}	888.8	15
v‴	Ce^{4+}	898.0	19
u_o	Ce^{3+}	898.9	1
u	Ce^{4+}	900.7	13
u′	Ce^{3+}	903.1	2
u″	Ce^{4+}	907.3	8
u‴	Ce^{4+}	916.6	14

Figure captions

Fig. 1. XPS of Ce3d core levels in as-deposited CeO_2 thin films on (a) Si and (b) Si_3N_4 substrates.

Fig. 2. Deconvoluted XPS of Ce3d core levels in as-deposited CeO_2 thin films on (a) Si and Si_3N_4 substrates.

Fig. 3. XPS of Si2p core levels in (a) CeO_2 deposited on Si substrate and (b) pure Si substrate.

Fig. 4. Deconvoluted XPS of O1s core levels in as-deposited CeO_2 thin films on (a) Si and (b) Si_3N_4 substrates.

Fig. 5. XPS of Ce3d core levels in CeO_2 thin films with different conditions: (a) deposited on Si and heat treated at 400 °C in vacuum, (b) deposited on Si and heat treated at 600 °C in vacuum, (c) deposited on Si_3N_4 and heat treated at 400 °C in vacuum, (d) deposited on Si_3N_4 and heat treated at 400 °C in air, (e) deposited on Si_3N_4 and heat treated at 600 °C in vacuum, and (f) deposited on Si_3N_4 and heat treated at 600 °C in air.

Fig. 6. Deconvoluted XPS of Ce3d core levels in CeO_2 thin films deposited on (a) Si substrate and heat treated at 400 in vacuum and (b) Si_3N_4 substrate and heat treated at 600 °C in vacuum.

Fig. 7. XPS of Ce4d core levels in CeO_2 thin films with different conditions: (a) as-deposited on Si, (b) as-deposited on Si_3N_4, (c) deposited on Si and heat treated at 400 °C in vacuum, (d) deposited on Si and heat treated at 600 °C in vacuum, (e) deposited on Si_3N_4 and heat treated at 400 °C in vacuum, (f) deposited on Si_3N_4 and heat treated at 400 °C in air, (g) deposited on Si_3N_4 and heat treated at 600 °C in vacuum, and (h) deposited on Si_3N_4 and heat treated at 600 °C in air.

Fig. 8. Deconvoluted XPS of Si2p core levels in CeO_2 thin films on Si substrate heat treated at (a) 400 and (b) 600 °C in vacuum.

Fig. 9. XPS of Si2p core levels in CeO_2/Si_3N_4 thin films with different conditions: (a) pure Si_3N_4, (b) as-deposited, (c) heat treated at 400 °C in vacuum, (d) heat treated at 400 °C in air, (e) heat treated at 600 °C in vacuum, and (f) heat treated at 600 °C in air.

Fig. 10. Deconvoluted XPS of O1s core levels in (a) CeO_2/Si and (b) CeO_2/Si_3N_4 thin films after heat treatment at 400 °C in vacuum.

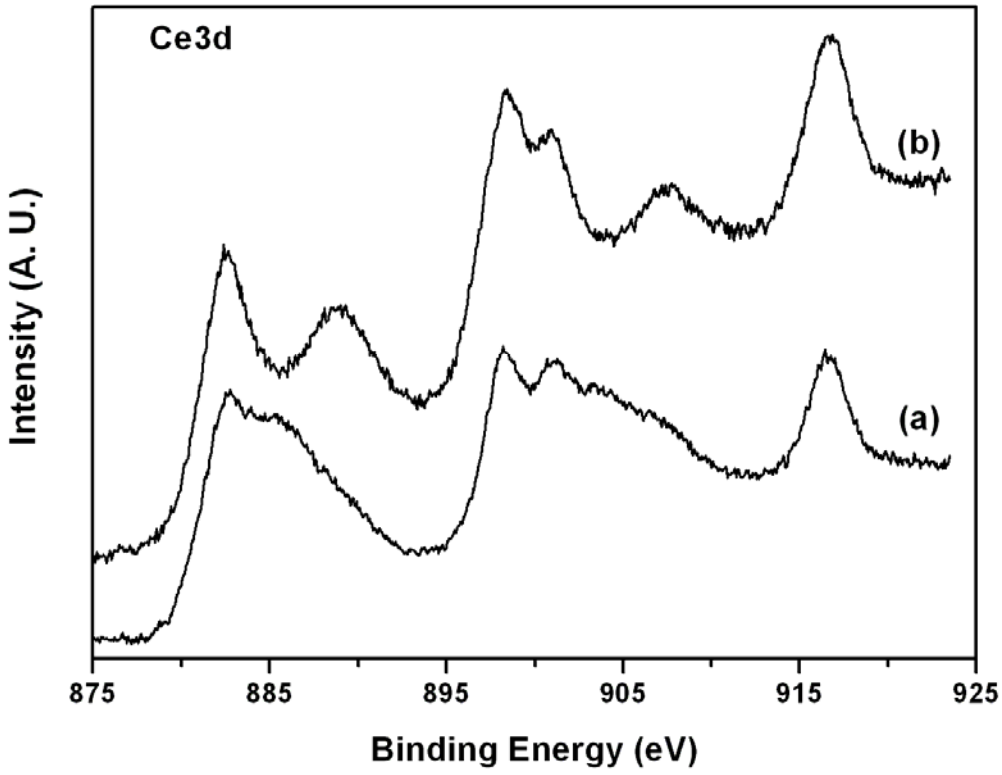

Fig. 1. XPS of Ce3d core levels in as-deposited CeO_2 thin films on (a) Si and (b) Si_3N_4 substrates.

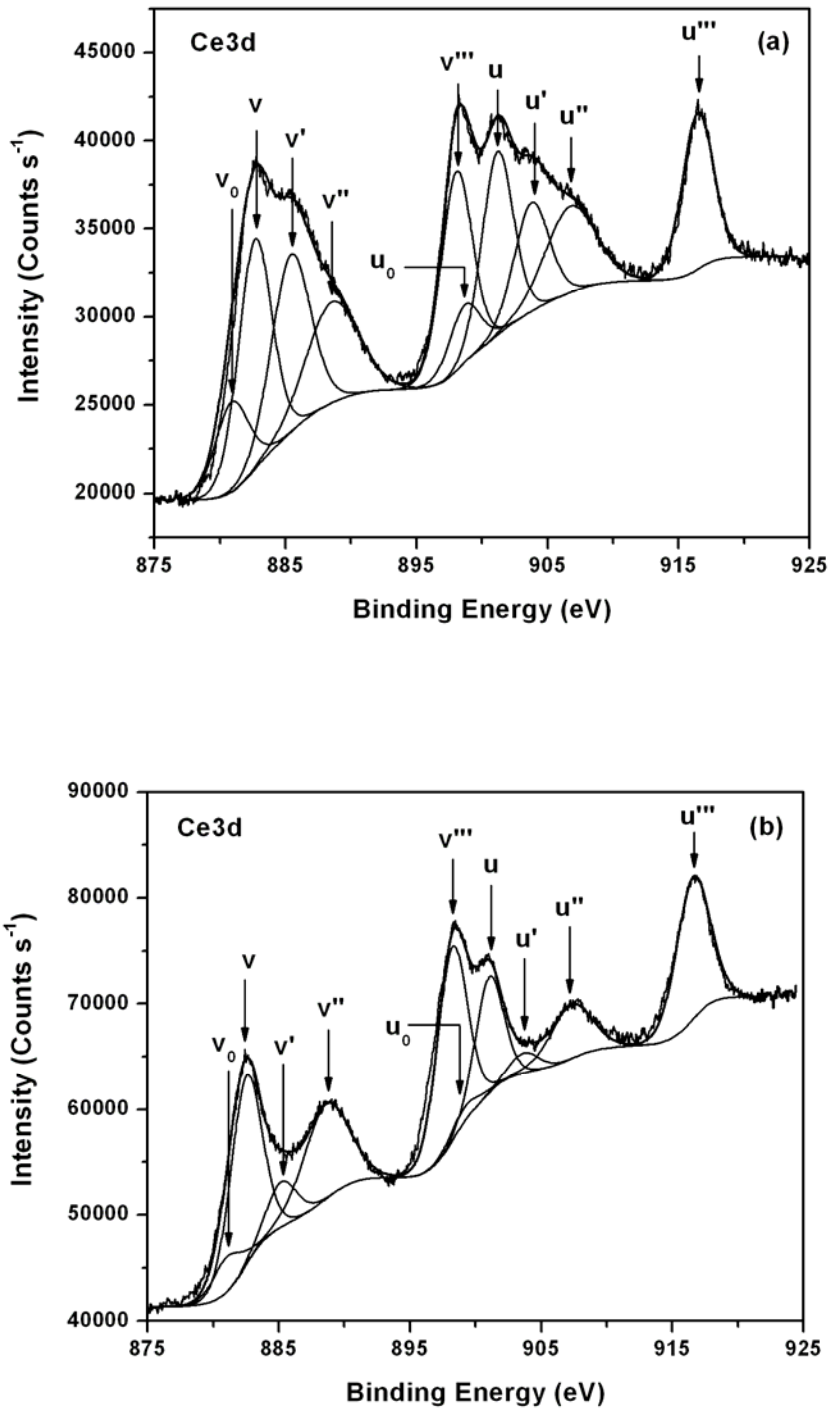

Fig. 2. Deconvoluted XPS of Ce3d core levels in as-deposited CeO_2 thin films on (a) Si and Si_3N_4 substrates.

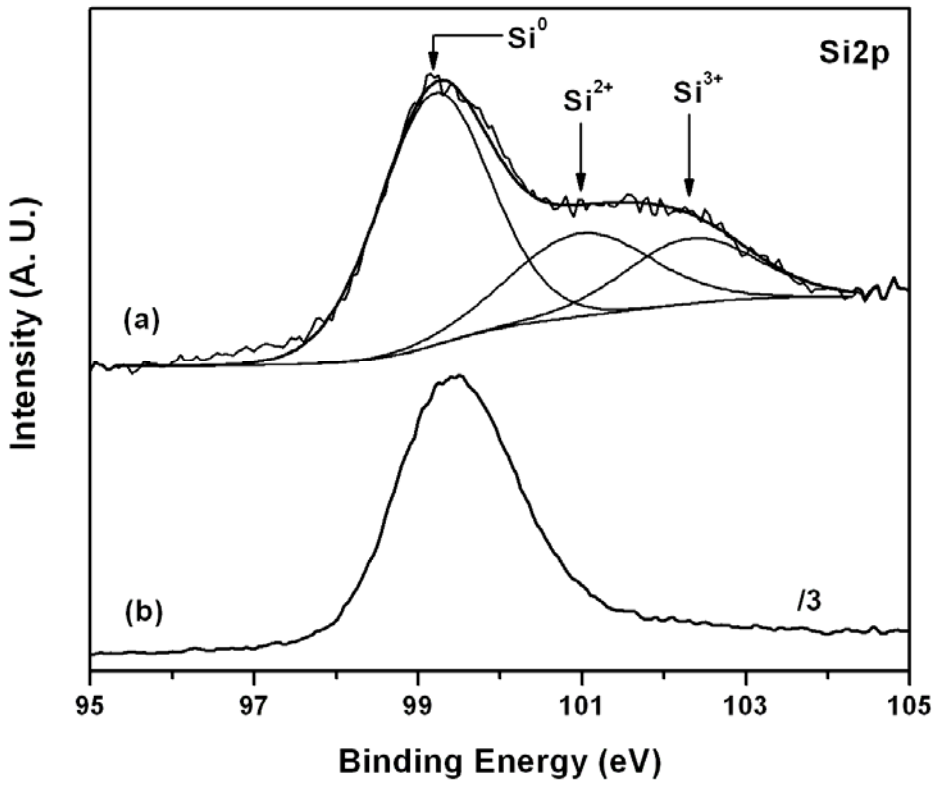

Fig. 3. Deconvoluted XPS of Si2p core levels in (a) CeO_2 deposited on Si substrate and (b) pure Si substrate.

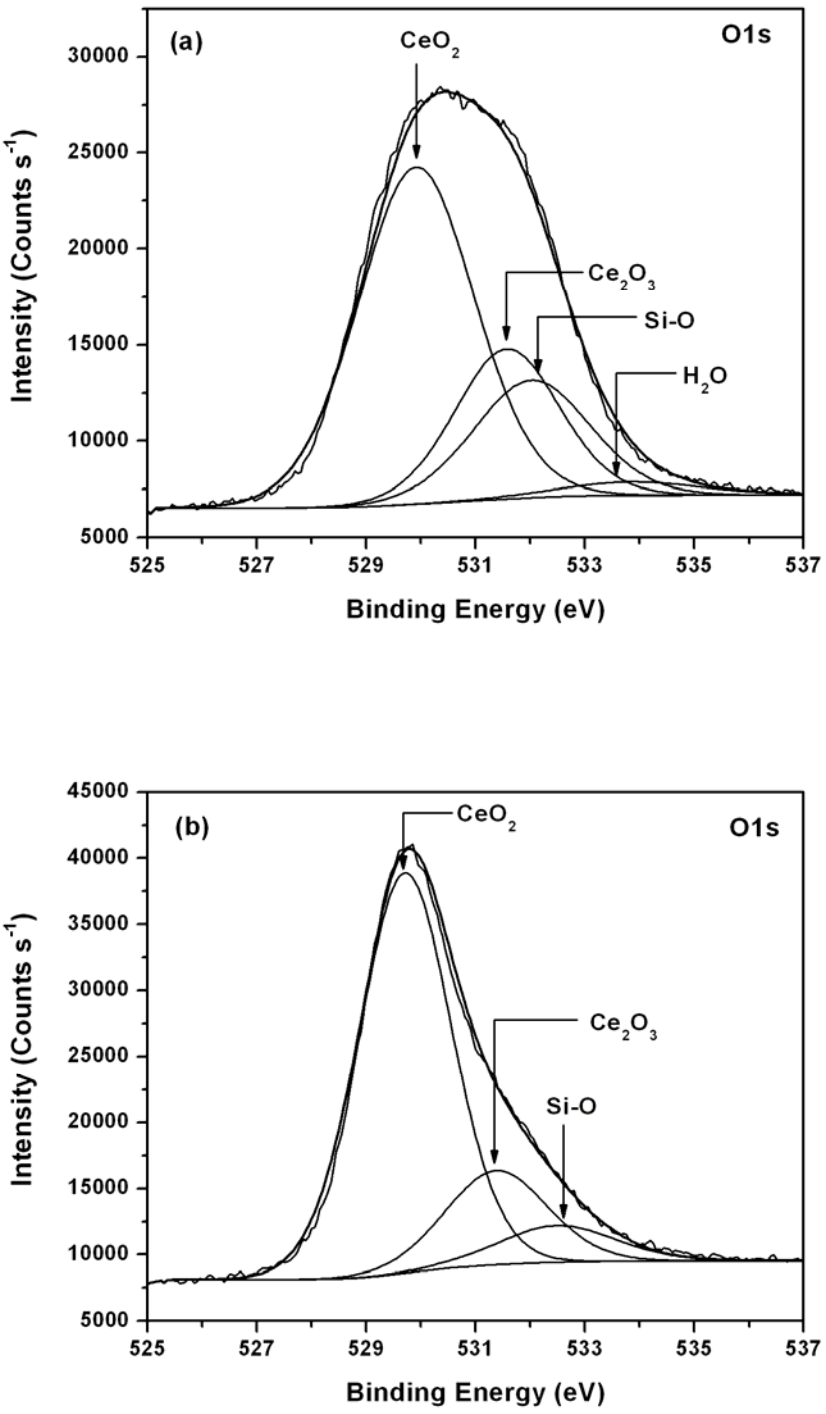

Fig. 4. Deconvoluted XPS of O1s core levels in as-deposited CeO_2 thin films on (a) Si and (b) Si_3N_4 substrates.

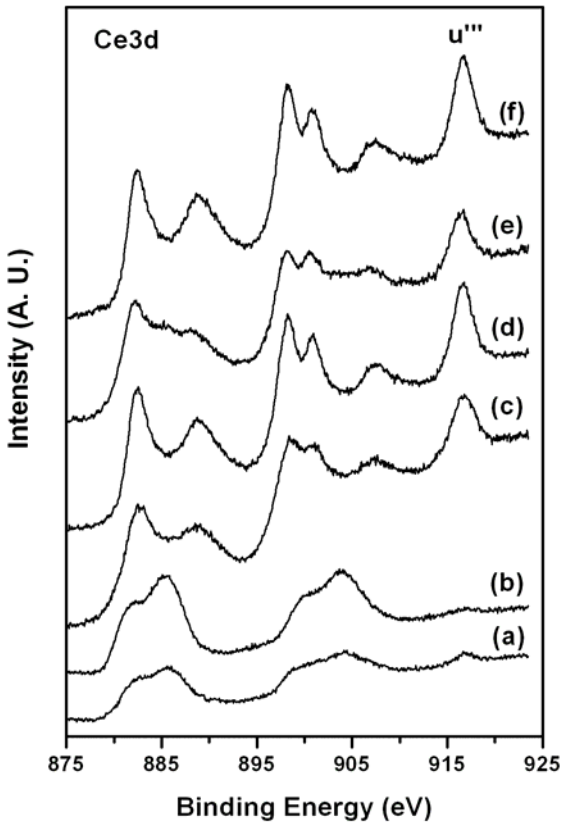

Fig. 5. XPS of Ce3d core levels in CeO_2 thin films with different conditions: (a) deposited on Si and heat treated at 400 °C in vacuum, (b) deposited on Si and heat treated at 600 °C in vacuum, (c) deposited on Si_3N_4 and heat treated at 400 °C in vacuum, (d) deposited on Si_3N_4 and heat treated at 400 °C in air, (e) deposited on Si_3N_4 and heat treated at 600 °C in vacuum, and (f) deposited on Si_3N_4 and heat treated at 600 °C in air.

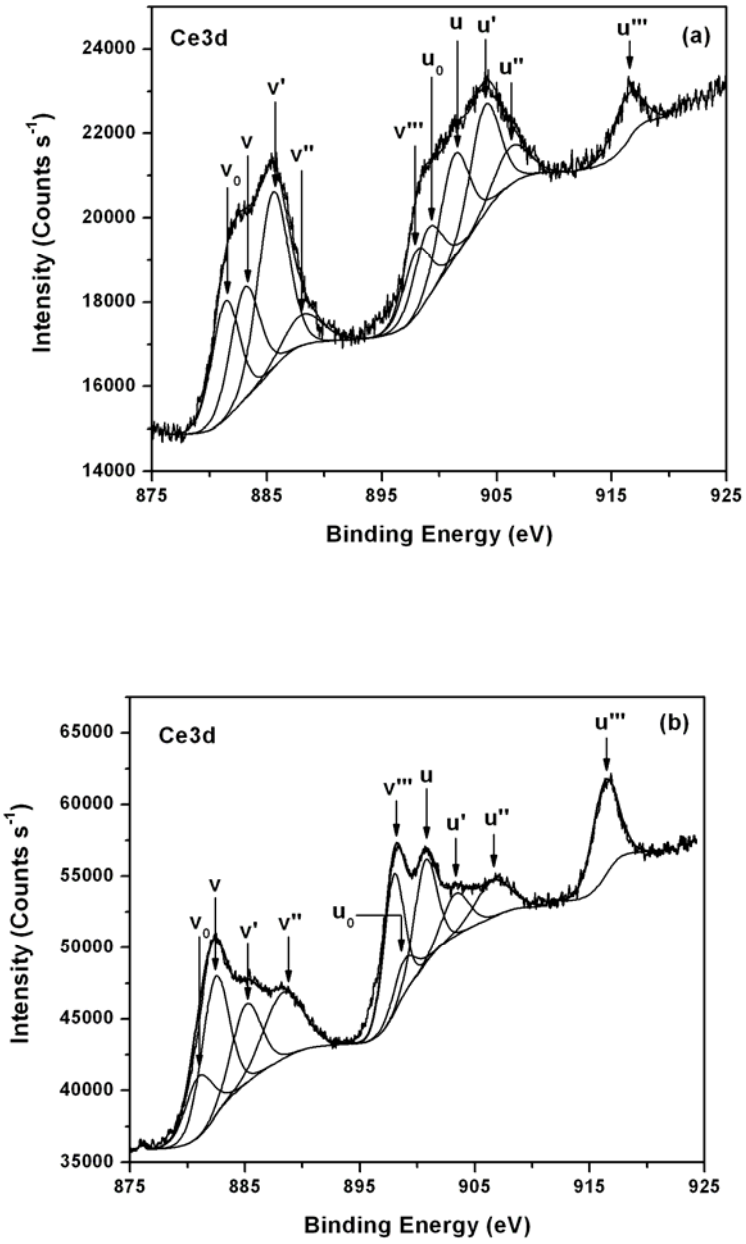

Fig. 6. Deconvoluted XPS of Ce3d core levels in CeO_2 thin films deposited on (a) Si substrate and heat treated at 400 in vacuum and (b) Si_3N_4 substrate and heat treated at 600 °C in vacuum.

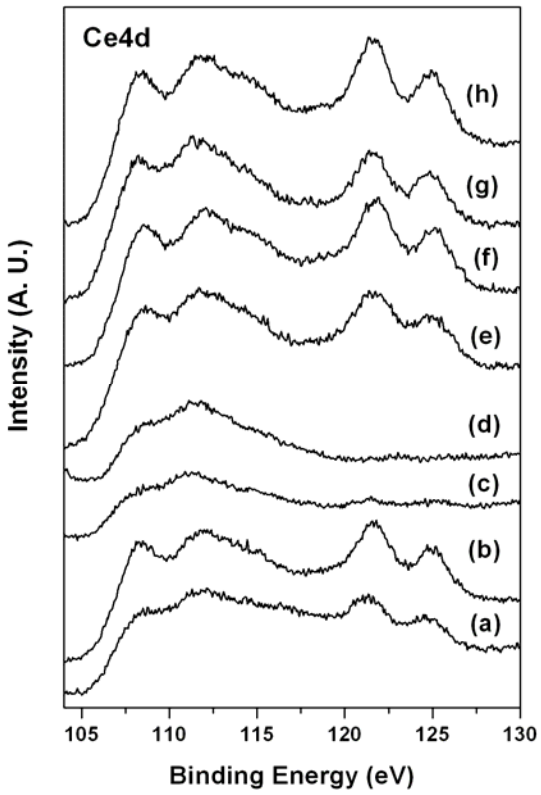

Fig. 7. XPS of Ce4d core levels in CeO_2 thin films with different conditions: (a) as-deposited on Si, (b) as-deposited on Si_3N_4, (c) deposited on Si and heat treated at 400 °C in vacuum, (d) deposited on Si and heat treated at 600 °C in vacuum, (e) deposited on Si_3N_4 and heat treated at 400 °C in vacuum, (f) deposited on Si_3N_4 and heat treated at 400 °C in air, (g) deposited on Si_3N_4 and heat treated at 600 °C in vacuum, and (h) deposited on Si_3N_4 and heat treated at 600 °C in air.

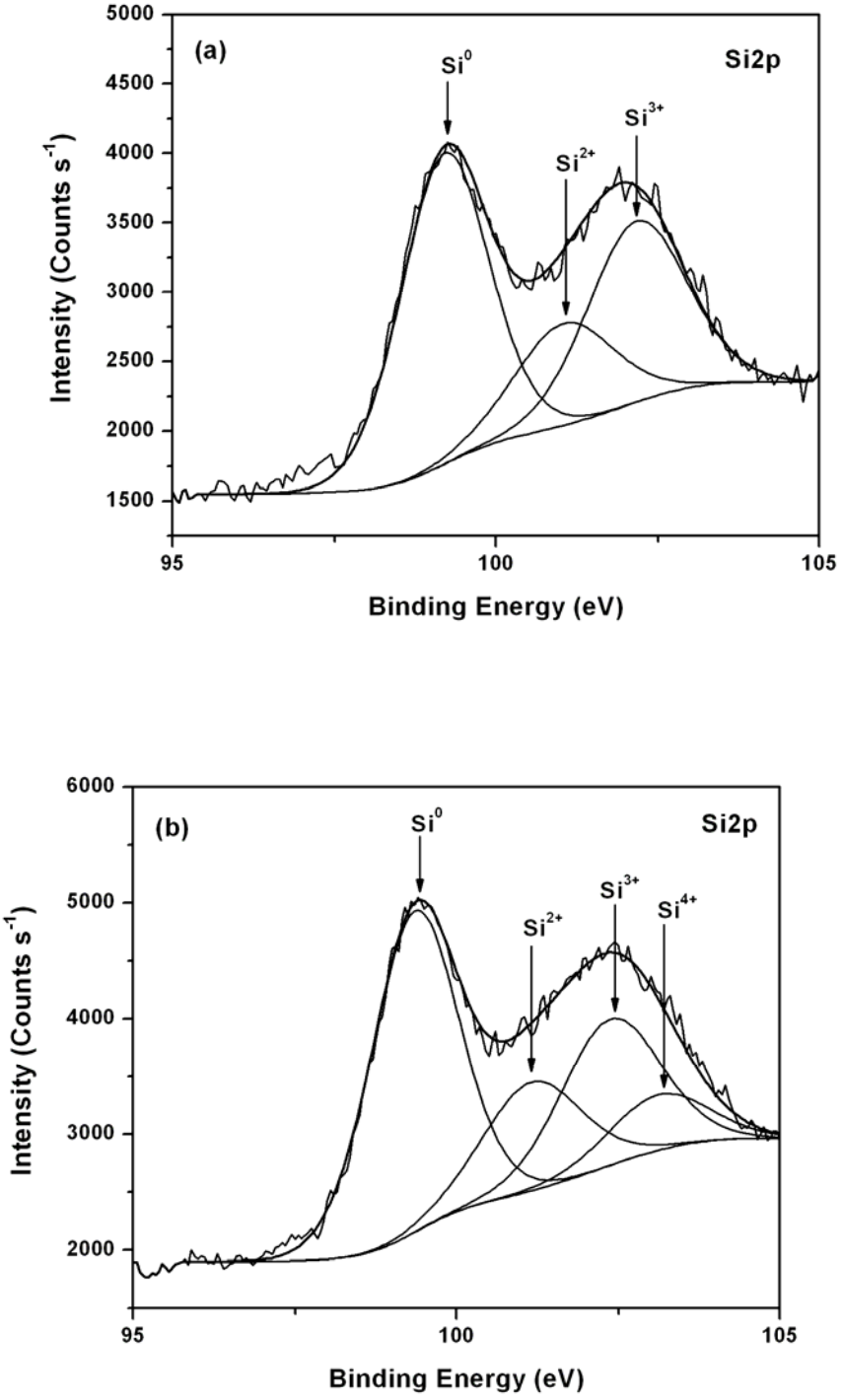

Fig. 8. Deconvoluted XPS of Si2p core levels in CeO_2 thin films on Si substrate heat treated at (a) 400 and (b) 600 °C in vacuum.

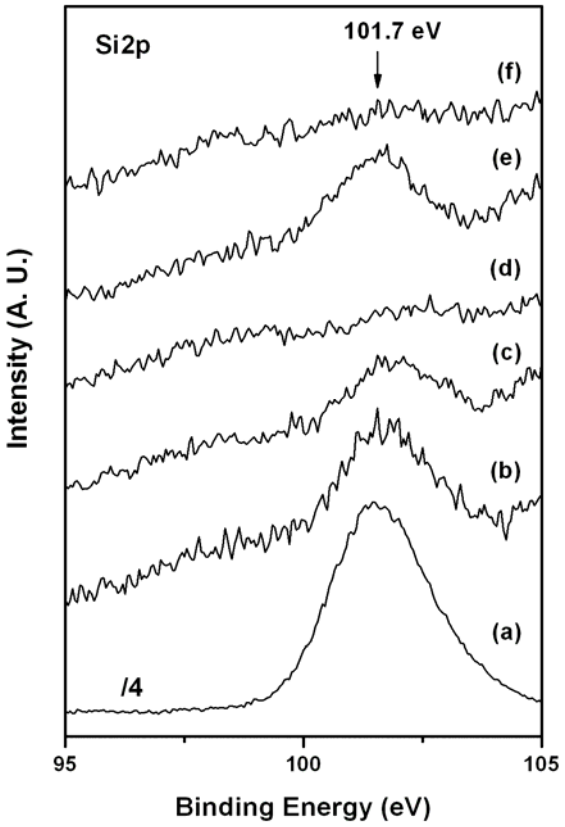

Fig. 9. XPS of Si2p core levels in CeO_2/Si_3N_4 thin films with different conditions: (a) pure Si_3N_4, (b) as-deposited, (c) heat treated at 400 °C in vacuum, (d) heat treated at 400 °C in air, (e) heat treated at 600 °C in vacuum, and (f) heat treated at 600 °C in air.

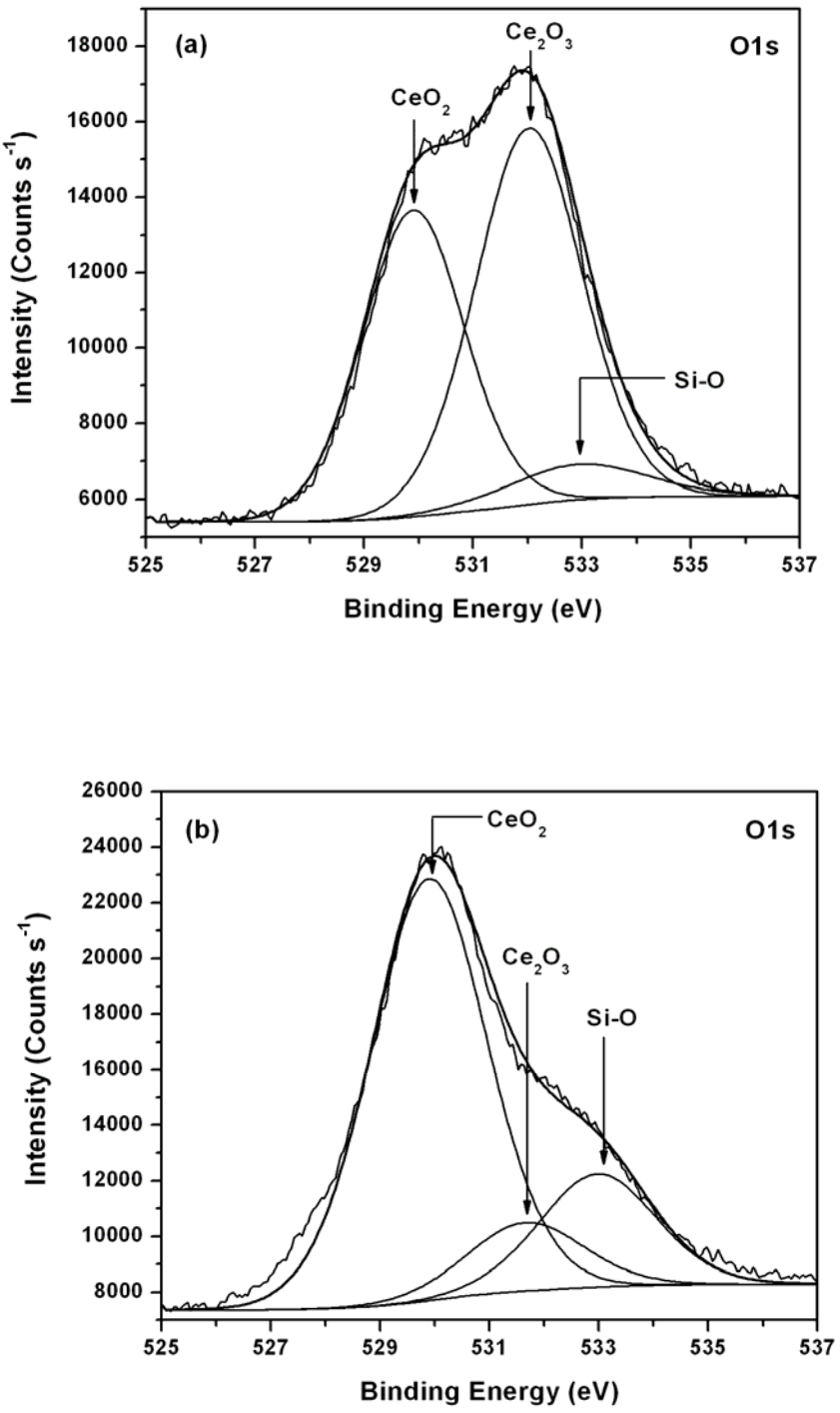

Fig. 10. Deconvoluted XPS of O1s core levels in (a) CeO_2/Si and (b) CeO_2/Si_3N_4 thin films after heat treatment at 400 °C in vacuum.